ORIGINAL PAPER

Preparation, molecular structure, thermal properties, electrical conductivity analysis and dielectric relaxation of a new hybrid compound (NH$_2$C$_5$H$_3$ClNH)$_2$ZnBr$_4$·H$_2$O

Besma Hamdi[1] · Ridha Zouari[1] · Abdelhamid Ben Salah[1]

Abstract

Preparation, structural elucidation, Hirshfeld surface analysis, thermal analysis and impedance spectroscopy study are carried out for an interesting organic–inorganic hybrid compound (NH$_2$C$_5$H$_3$ClNH)$_2$ZnBr$_4$·H$_2$O. X-ray diffraction analysis reveals that the title compound belongs to the triclinic crystallographic system with the space group P-1 with $Z = 2$ and the following unit cell dimensions: $a = 7.3209(9)$ Å, $b = 8.4407(10)$ Å, $c = 16.923(2)$ Å, $\alpha(°) = 82.975(6)$, $\beta(°) = 85.118(6)$ and $\gamma(°) = 74.398(6)$. The crystal structure is composed of two protonated 4-amino-2-chloropyridinium cations, tetrabromozincate anions and a water molecule which are held together by a number of hydrogen bonds forming infinite chains. In addition, crystal structure is stabilized with π…π interactions (Cg–Cg and Zn-Cl…Cg, with Cg is the 4-amino-2-chloropyridinium rings) which have also been investigated in terms of their corresponding Hirshfeld surface and the breakdown of fingerprint. To quantify intermolecular interactions in crystal lattice, FT-IR spectroscopy has been used to distinguish the different chemical functional groups and their environments in this molecule. The dielectric conductivity of this compound has been measured in the temperature range 298–438 K and the frequency range 209 Hz–5 MHz. The analysis of the experimental data of the impedance spectroscopy based on the activation energy shows that this material is an ionic–protonic conductor at low temperature and becomes an electronic one at high temperature. This work aims to reveal the thermal properties of a new zinc (II) based organic–inorganic hybrid and the conductivity properties that this compound exhibits.

Keywords Chemical synthesis · X-ray diffraction · Hirshfeld surface · FT-IR · Thermal properties · Impedance spectroscopy

Introduction

Over decades of chemical research, preparations and characterizations of organic–inorganic metal-based bivalent cations are carried out by several researchers throughout the world attempting to combine desirable physical properties of both organic and inorganic components within a single molecular-scale composite. Among these compounds, we mention hybrids with cations. These compounds have attracted

the attention of researchers and whetted their interest, since they exhibit different kinds of phase transitions generally related to the motion of the alkyl ammonium cations (Karâa et al. 2010, 2013). Moreover, halogenozincate compounds are essentially associated with their potential applications and interesting electrical properties (Chihaoui et al. 2016a, b, 2017).

The organic divalent zinc chloride has several applications in various domains such as catalysis, biochemistry, dielectric transition and magnetism material science (Chihaoui et al. 2016a, b, 2017). In addition, the study of such zinc-based materials has received much attention recently in the light of photovoltaic and multifunctional properties. Besides, the organization of the interactions in the crystal packing plays a major role to advance diverse applications in industry. For this reason, we attempt to seek a novel structural topologies and properties that can be useful in the

✉ Besma Hamdi
bh_hamdi2006@yahoo.fr

1   Faculty of Sciences, Material and Environment Science Laboratory, University of Sfax, BP 1171, 3000 Sfax, Tunisia

field of luminescence and semiconductivity (Chihaoui et al. 2016a, b, 2017).

Having the motivations stated above and encouraged by this pioneering work, we attempt to present a novel hybrid compound: (4-amino-2-chloropyridinium)2 tetrabromozincate (II) monohydrate, $(NH_2C_5H_3ClNH)_2ZnBr_4 \cdot H_2O$. A detailed interpretation of the structural geometry of the crystal has been displayed. Further processes (Hirshfeld surface analyses) have been used to investigate the various contacts and the intermolecular interactions in the crystal packing analysis, which are derived by single-crystal XRD data and spectroscopic technique (FT-IR). Besides, thermal analysis (DSC and TGA) and careful examination of ionic conductivity of the compound have been performed. The electrical features of the material have been studied using complex impedance spectroscopy.

Experimental section

Synthesis and crystallization

All reagents were obtained commercially and used without further purifications. The first step of the preparation of the material was the preparation of 4-amino-2-chloropyridiniumbromide $((NH_2C_5H_3ClNH)^+, Br^-)$ solution which was formed through the addition of an aqueous solution of HBr (10 ml) to 4-amino-2-chloropyridine $(NH_2C_5H_3ClN)$ (2.5 mmol). The dried precipitates were then washed with diethyl ether to remove unreacted substances. The stoichiometric amounts 2:1 of the resulting solution $[(NH_2C_5H_3ClNH)^+, Br^-]$ and $ZnBr_2$ (1.25 mmol) were mixed with excess of HBr. The slow evaporation is the method used to obtain transparent crystals. The mixture was stirred and kept at room temperature for several days. Needle like transparent crystals were obtained a week later. A single crystal suitable for X-ray diffraction analysis was selected and studied.

Crystallography

A suitable single crystal with dimensions of $0.42 \times 0.39 \times 0.20$ mm^3 for $(NH_2C_5H_3ClNH)_2ZnBr_4 \cdot H_2O$ was selected for single-crystal X-ray diffraction analysis. The intensity data for the single crystal compound investigations was collected at 293(2) (K) using BRUKER AXS (Kappa APEX II-CCD area detector). The sample was selected under polarising microscope and examined by oscillation method. The intensity data was collected with Graphite monochromated MoKα radiation ($\lambda = 0.71073$ Å). The Zinc, Bromide and Chloride atoms were located by Patterson methods using SHELXS-97 (Sheldrick 1997). However, the organic entities were found from successive Fourier calculations and refined through the full-matrix

least-squares method using SHELXL-97 (Sheldrick 1997), implemented in the WinGX (Farrugia 1999) software package. Crystal parameters and details of data collection are presented in Table 1. The final atomic coordinates obtained from the single crystal refinement with Ueq are displayed in table S1. Anisotropic thermal displacement parameters were used to refine all non-hydrogen atoms, shown in table S2. Hydrogen atoms of the organic ring and water were fixed at their ideal positions. The final geometrical calculations and the graphical manipulations were carried out with ORTEP (Farrugia 1997), MERCURY (Spek 2003) and DIAMOND (Brandenburg 1998) programs. Selected bond lengths and angles are exhibited in Table 2. Data for the structure of $(NH_2C_5H_3ClNH)_2ZnBr_4 \cdot H_2O$ can be obtained free of charge from the Cambridge Crystallographic Data Center http://www.ccdc.cam.ac.uk/conts/retrieving.html (or from the Cambridge Crystallographic Data Center, 12 Union Road, Cambridge CB2 1EZ, UK; fax: (+44) 1223-336-033; or e-mail: deposit@ccdc.cam.ac.uk), with CCDC reference numbers 1577208 containing the supplementary crystallographic data for this paper.

Hirshfeld surfaces calculations

To further understand the atomic interactions in the crystal structure, we have determined the Molecular Hirshfeld surfaces (Spackman and McKinnon 2002) which are constructed on the basis of electron distribution calculated as the sum of spherical atom electron densities (Spackman and Byrom 1997). The CrystalExplorer 3.1 program (Wolff et al. 2012) was used to construct the three-dimensional Hirshfeld surfaces as well as the fingerprint plots.

The d_{norm} (normalized contact distance) is a symmetric function of distances which are the nearest nuclei internal and external to the Hirshfeld surface (d_i and d_e, respectively), relative to their respective *van der Waals radii* of the atoms internal or external to the surface (r_i^{vdw}/r_e^{vdw}) which identifies the regions of particular importance to the intermolecular interactions given by the following equation:

$$d_{norm} = \{(d_i - r_i^{vdw})/r_i^{vdw}\} + \{(d_e - r_e^{vdw})/r_e^{vdw}\}, \qquad (1)$$

with r_i^{vdw} and r_e^{vdw} being the *van der Waals* radii of the respective atoms which are internal and external to the molecular surface.

In the color scale, negative values of d_{norm} are detected through the red color, indicating contacts shorter than the sum of *van der Waals* radii. The white color denotes intermolecular distances close to *van der Waals* contacts with d_{norm} equal to zero. In turn, contacts longer than the sum of *van der Waals* radii with positive d_{norm} values are indicated by blue. Two colored properties (shape-index and curvedness) based on the local curvature of the surface can be specified (Koenderink and van Doorn 1992).

Table 1 Summary of crystal data, intensity measurements and refinement parameters for $(NH_2C_5H_3ClNH)_2ZnBr_4 \cdot H_2O$ crystal

Crystal data	
Empirical formula	$(NH_2C_5H_3ClNH)_2ZnBr_4 \cdot H_2O$
Formula weight	662.14
Crystal system	Triclinic
Space group	P-1
Hall symbol	-P 1
Unit cell dimensions	
a (Å)	7.3209(9)
b (Å)	8.4407(10)
c (Å)	16.923(2)
α (°)	82.975(6)
β (°)	85.118(6)
γ (°)	74.398(6)
Volume (Å³)	998.2(2)
Z	2
D_{calc} (mg m⁻³)	2.203
Absorption coefficient (mm⁻¹)	9.507
$F(000)$	628
Crystal dimensions (mm)	$0.42 \times 0.39 \times 0.20$
Crystal color	Transparent crystals
θ range for data collection (°)	1.21–30.45
Data collection	
Reflections collected	14,338
Independent reflections	4860
Reflections with $I > 2\sigma(I)$	2086
	$h = -10 \rightarrow 10$
	$k = -10 \rightarrow 12$
	$l = -23 \rightarrow 22$
Absorption correction	$T_{min} = 0.024$
	$T_{max} = 0.151$
	Multi-scan (North et al. 1968)
Refinement	
Refinement method	Full-matrix least squares on F^2
$R [F^2 > 2r(F^2)]$	0.046
$wR(F^2)$	0.0787
Goodness-of-fit on F^2	$S = 0.912$
CCDC deposit number	**1577208**
CCD area detector diffractometer radiation	
Source: fine-focus sealed	
Tube graphite φ and ω scans	

Primary atom site location: structure-invariant direct methods; secondary atom site location: difference Fourier map. Hydrogen site location: inferred from neighboring sites H-atom parameters constrained

$w = 1/[\sigma^2(Fo^2) + (0.0377P)^2 + 0.0000P]$ where $P = (Fo^2 + 2Fc^2)/3$. Extinction correction: SHELXL

Table 2 Main distances (Å) and bond angles (°) in the $(NH_2C_5H_3ClNH)_2ZnBr_4 \cdot H_2O$ crystal (e.s.d. are given in parentheses)

Distances (Å)		Angles (°)	
Tetrahedron $[ZnBr_4]^{2-}$			
Br_1–Zn_1	2.4174 (11)	Br_4–Zn_1–Br_3	106.52 (4)
Br_2–Zn_1	2.4197 (11)	Br_4–Zn_1–Br_1	111.41 (4)
Br_3–Zn_1	2.4095 (11)	Br_3–Zn_1–Br_1	108.25 (4)
Br_4–Zn_1	2.4003 (10)	Br_4–Zn_1–Br_2	110.48 (4)
		Br_3–Zn_1–Br_2	111.50 (4)
		Br_1–Zn_1–Br_2	108.67 (4)
1st organic molecule			
Cl_1–C_3	1.716 (7)	C_3–N_1–C_2	119.6 (6)
C_1–C_2	1.340 (9)	C_5–C_3–Cl_1	122.3 (6)
C_1–C_4	1.412 (9)	N_1–C_3–Cl_1	115.8 (6)
N_1–C_3	1.342 (8)	N_2–C_4–C_5	123.0 (7)
		N_2–C_4–C_1	119.8 (7)
$N1$–$C2$	1.347 (8)	C_5–C_4–C_1	117.2 (6)
$N2$–$C4$	1.324 (8)	C_3–C_5–C_4	120.2 (7)
$C3$–$C5$	1.330 (8)	C_2–C_1–C_4	119.4 (7)
$C4$–$C5$	1.400 (8)	C_1–C_2–N_1	121.8 (7)
		C_5–C_3–N_1	121.8 (6)
2nd organic molecule			
C_6–C_7	1.331 (8)	C_8–N_3–C_7	119.0 (6)
C_6–C_{10}	1.416 (9)	C_7–C_6–C_{10}	119.0 (6)
C_8–C_9	1.334 (8)	C_6–C_7–N_3	122.2 (7)
C_9–C_{10}	1.417 (9)	C_6–C_7–Cl_2	122.1 (5)
N_4–C_{10}	1.362 (8)	N_3–C_7–Cl_2	115.7 (5)
N_3–C_7	1.352 (8)	C_9–C_8–N_3	123.6 (6)
N_3–C_8	1.339 (8)	N_4–C_{10}–C_9	119.9 (7)
Cl_2–C_7	1.711 (7)	C_8–C_9–C_{10}	117.9 (7)
		N_4–C_{10}–C_6	121.8 (6)
		C_6–C_{10}–C_9	118.3 (6)
Water molecule			
O_1–H_1B	0.8500	H_1B–O_1–H_1C	109.50
O_1–H_1C	0.8500		

Thermal analysis

The DSC calorimetric measurement was carried out using a Perkin Elmer PYRIS 6 DSC calorimeter, by putting a powder sample (about 9.06 mg) in an aluminum capsule. The DSC was performed with a heating rate of 5 K/min up to 430 K under constant nitrogen flow.

Thermogravimetric analysis (TGA) was carried out using an ATG PYRIS 6 instrument with a heating rate of 5 K/min up to 430 K under a nitrogen atmosphere.

FT-IR spectroscopy

The infrared absorption spectrum (FT-IR) (Fig. 4) (spectrum in red) of the crystallized powder

Fig. 1 View of the asymmetric unit of $(NH_2C_5H_3ClNH)_2ZnBr_4 \cdot H_2O$ showing the atom-labeling scheme. Displacement ellipsoids are drawn at the 50% probability level

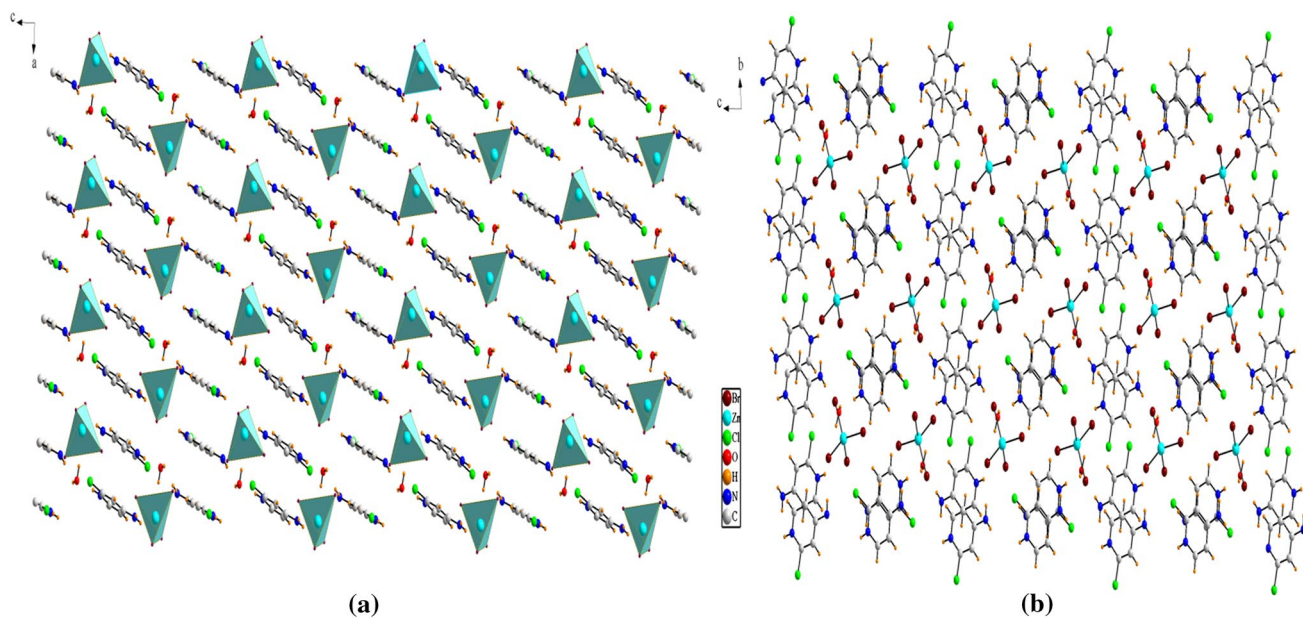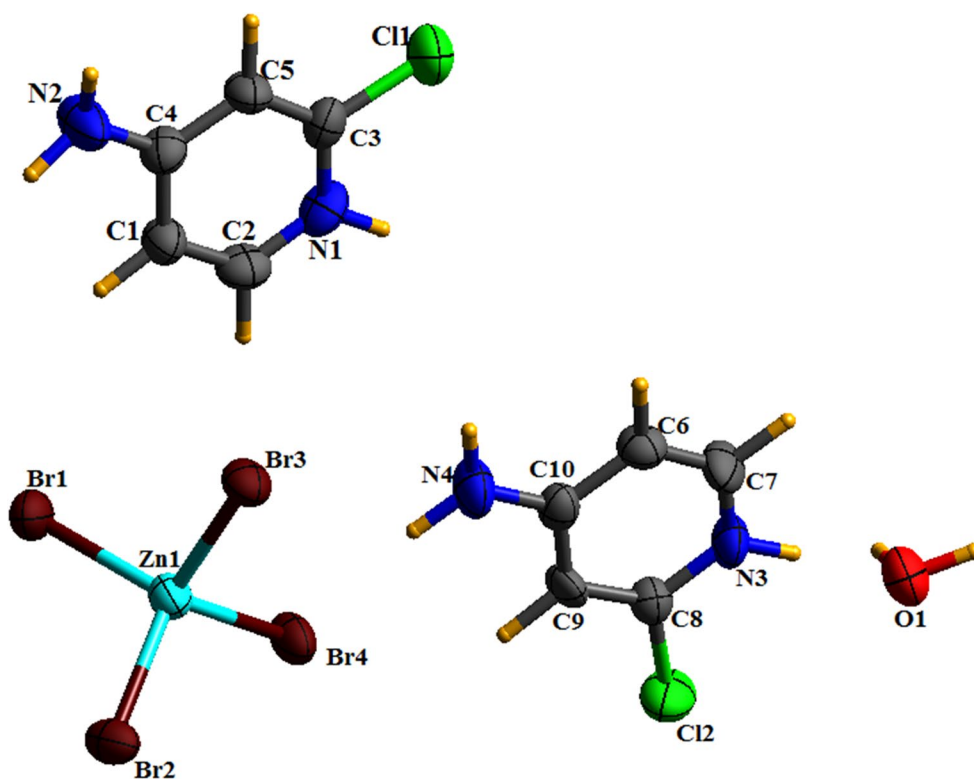**Fig. 2** Projection of the atomic arrangement of $(NH_2C_5H_3ClNH)_2ZnBr_4 \cdot H_2O$ structure; **a**: along *b* axis; **b**: along *a* axis

$(NH_2C_5H_3ClNH)_2ZnBr_4 \cdot H_2O$, was recorded on a Nicolet Impact 410 spectrometer in the 4000–400 cm^{-1} range at room temperature. The measurement is carried out on a pellet containing 95% of KBr and 5% of powder.

Electrical impedance spectroscopy

The impedance spectroscopy was performed on pellet discs of about 8 mm diameter and about 1.6 mm in thickness. Electrical impedances were measured in the frequency range

Fig. 3 The image showing the intermolecular hydrogen bond contacts for $(NH_2C_5H_3ClNH)_2ZnBr_4 \cdot H_2O$ (represented by dotted lines)

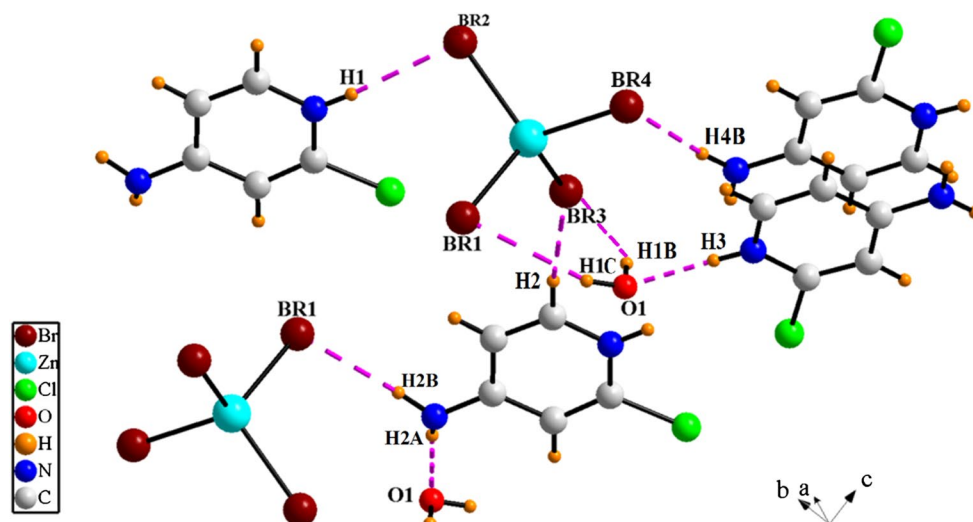**Table 3** Main inter–atomic distances (Å) and bond angles (°) involved in the hydrogen bonds of $(NH_2C_5H_3ClNH)_2ZnBr_4 \cdot H_2O$ crystal

D–H…A	D–H	H…A	D…A	D–H…A
N_1–H_1…Br_2	0.8600	2.5100	3.3665	173.00
O_1–H_1B…Br_3	0.8500	2.8400	3.4491	130.00
O_1–H_1C…Br_1	0.8500	2.7800	3.5327	148.00
N_2–H_2A…O_1	0.8600	2.1600	2.9721	158.00
N_2–H_2B…Br_1	0.8600	2.6100	3.4622	172.00
N_3–H_3…O_1	0.8600	1.9200	2.7798	178.00
N_4–H_4B…Br_4	0.8600	2.6700	3.5300	175.00
C_2–H_2…Br_3	0.9300	2.7800	3.6959	170.00

from 209 Hz to 5 MHz with the TEGAM 3550 ALF automatic bridge over a temperature range of (298–438 K).

Results and discussion

Structure description

The structure of a new compound was developed in the centro-symmetric space group P-1 with ($Z=2$), with the following unit cell dimensions: $a = 7.3209(9)$ Å, $b = 8.4407(10)$ Å, $c = 16.923(2)$ Å, $\alpha(°) = 82.975(6)$, $\beta(°) = 85.118(6)$, $\gamma(°) = 74.398(6)$ and $v = 998.2(2)$ Å^3. The asymmetric unit of the structure drawn with 50% probability thermal ellipsoids and exposed in Fig. 1 shows the ORTEP drawing of the asymmetric unit together with an atom numbering scheme (Farrugia et al. 1997). As it can be noticed, the asymmetric unit of the title compound comprises two crystallographically independent organic cations denoted 4-amino-2-chloropyridinium

$[(NH_2C_5H_3ClNH)^+(I)$ and $(NH_2C_5H_3ClNH)^+(II)]$ protonated cations ligand, one $[ZnBr_4]^{2-}$ anion and one uncoordinated water molecule. The hybrid organic–inorganic compound $(NH_2C_5H_3ClNH)_2ZnBr_4 \cdot H_2O$ naturally forms a periodic zero-dimensional structure which consists of alternating layers of organic and inorganic corrugated sheets stacked along *b* and *a* axis, as shown in Fig. 2. The graphical representation is provided with Diamond (Brandenburg 1998).

The zinc atom is tetrahedrally coordinated by bromine atoms; present in a slight distorted tetrahedral geometry. These slight distortions are usually determined by the angles Br–Zn–Br, varying between 106.52(4) and 111.50(4). The Zn–Br bond lengths are in the range 2.4003(10)–2.4197(11) Å. A full list of bond lengths and angles is given in Table 2. The bond distances and angles fall in the range of those reported previously for compounds containing Zn–Br anions (Gao et al. 2007; Chihaoui et al. 2016a, b, c).

The organic part consists of two organic cations; $(NH_2C_5H_3ClNH)^+$, each of which with an N ring site protonated, and carbon atoms building up the pyridine rings. These organic cations exhibit a regular spatial configuration with normal distances C–C, C–N and angles C–C–C, C–C–N and have a good co-planarity with similar compounds in our previous study results (Karâa et al. 2010, 2013). The N-pyridine atom with its hydrogen atoms lie in the plane of the ring. Both H atoms of the amino group and the N-pyridine are involved in hydrogen bonds.

Water oxygen, instead, forms two N–H…OH-bonds. The N–H…OH-bonding geometries are N…O distances from 2.9721 to 2.7798 Å and N–H…O angles from 158° to 178°. The number of H-bonds per formula is eight (Fig. 3; Table 3).

The structural analysis reveals that the stabilization of the whole supra-molecular assembly has been built up by two classes of contacts: the hydrogen bonds and π–π interactions.

Table 4 Analysis of short ring-interactions with π…π between the different organic molecules as well as Y–X…Cg (π–ring) interactions using PLATON

Analysis of short ring-interactions with Cg–Cg distances < 6.0 Å and β < 60.0 (°)				
Cg(I)…Cg(J)	Cg–Cg	α (°)	β (°)	γ (°)
Cg(1)…Cg(1)	5.1439	0	49.5	49.5
Cg(1)…Cg(1)	3.8180	0	26.1	26.1
Cg(2)…Cg(2)	4.7879	0	44.3	44.3
Cg(2)…Cg(2)	3.6673	0	20.8	20.8
Analysis of Y–X…Cg (π-Ring) interactions [X…Cg < 4.0 Å-γ < 30.0(°)]				
Y–X(I)…Cg(J)	X…Cg	γ (°)	Y–X…Cg	Y…Cg
Zn(1)–Br(1)…Cg(1)	3.8520	26.70	173	6.2583

Centroid Cg(1): ring (1): N(1)–C(2)–C(1)–C(4)–C(5)–C(3)

Centroid Cg(2): ring (2): N(3)–C(7)–C(6)–C(10)–C(9)–C(8)

Cg(I) Plane number I (ring number in (°) above)

α: dihedral angle between planes I and J (°)

β: angle Cg(I)–Cg(J) vector normal to plane I (°)

γ: angle Cg(I)–Cg(J) vector normal to plane J (°)

Cg–Cg: distance between ring centroids (Å)

Cg(I)-Perp: perpendicular distance of Cg(I) on ring J (Å)

Cg(J)-Perp: perpendicular distance of Cg(J) on ring I (Å)

Fig. 4 Alternating rows of π…π between the different organic molecules and Zn-Br1…Cg1 stacking interactions using PLATON
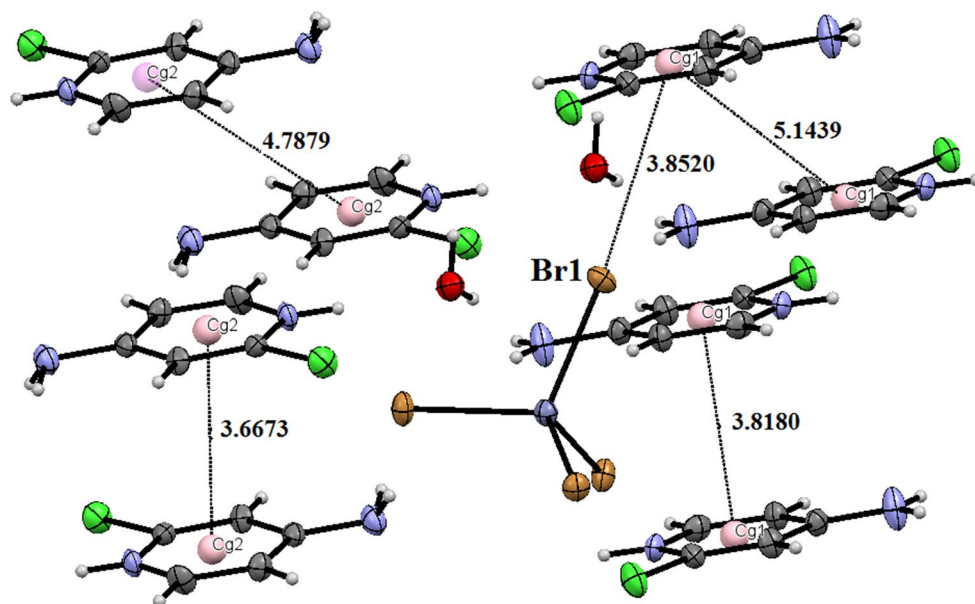
All hydrogen bondings are summarized in Table 3. A packing diagram (Fig. 3) of $(NH_2C_5H_3ClNH)_2ZnBr_4 \cdot H_2O$ structure shows the presence of various hydrogen bonds between the organic cation and the bromine atoms of the inorganic part which are linked by classic bonds (N–H… Br) involving the hydrogen atoms of NH (pyridin) and NH_2 (amine group). Other classical hydrogen bonds (C–H…Br) relate the carbon atom (α carbon: linked to the N-pyridine

atom) to the bromine atoms of $[ZnBr_4]^{2-}$. It can be noted from Fig. 3 that water molecules play a significant role in stabilizing the crystal structure. First, they are connected to $[ZnBr_4]^{2-}$ tetrahedral by O–H…Br bonding. Second, they are attached to the cationic part by N–H…O contact.

There are π–π stacking interactions between the 4-amino-2-chloropyridinium rings (Gillon et al. 2000, Ninković et al. 2012). The analysis of ring-interactions using PLATON

Fig. 5 Hirshfeld surfaces of cationic part in the asymmetric unit of $(NH_2C_5H_3ClNH)_2ZnBr_4 \cdot H_2O$ compound, showing views of d_{norm} (**a**), shape index (**b**), curvedness (**c**), and 2D fingerprint plot (**d**)
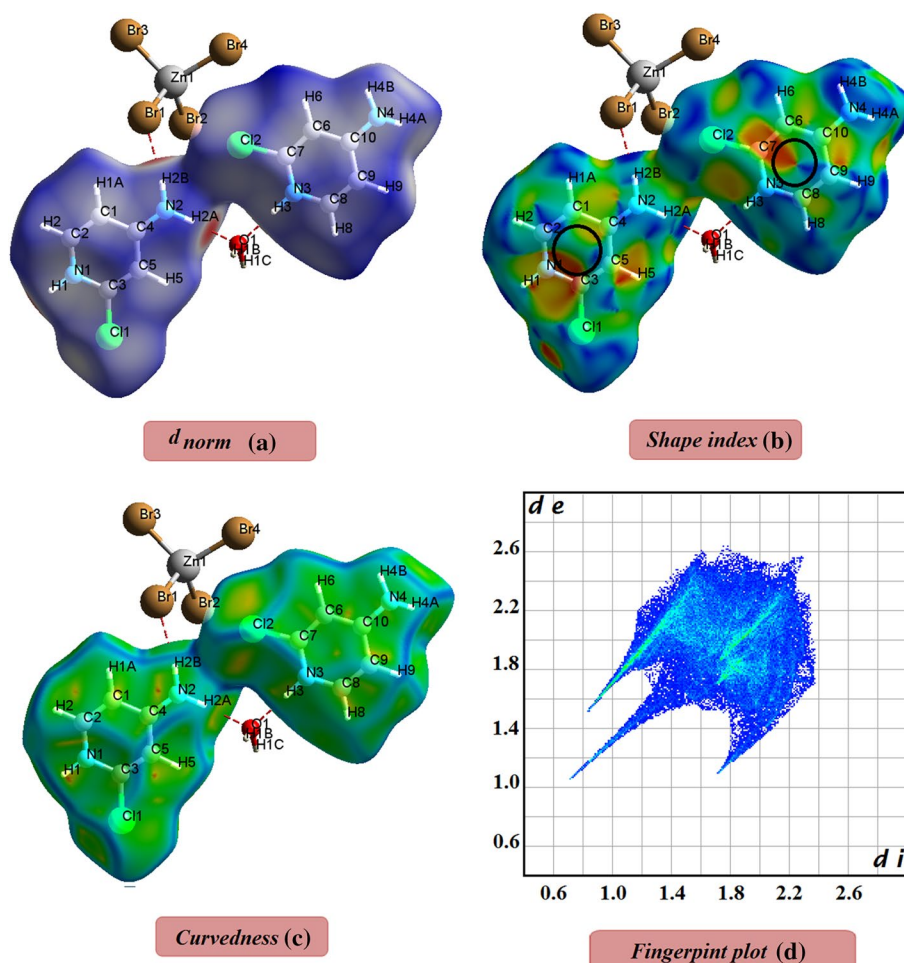
(Table 4; Fig. 4) (Spek 2003), shows that the rings' layers are parallel in the crystal connected with *van der Waals* forces. Stacking parameters which are taken into account are $d_{Cg1–Cg1}$ and $d_{Cg2–Cg2}$ (centroid–centroid distance), α (angle between planes containing aromatic rings), slipping angles β and γ (defined by the vector Cg–Cg and the normal to planes [Cg_1 corresponding to $(NH_2C_5H_3ClNH)^+(I)$] and [Cg_2 representing $(NH_2C_5H_3ClNH)^+(II)$]. Data of Table 4 reveals that $(NH_2C_5H_3ClNH)^+$ rings fall parallel ($\alpha = 0.00°$) at 3.6673–5.1439 Å. However, there are four interactions ring–ring π–π between the (4-amino-2-chloropyridinium) of the title compound (Fig. 4) (Wheeler 2012). On the other side, data in Table 4 shows possibilities for such M–X...π stacking lone pair of X (bromide) and 4-amino-2-chloropyridinium rings, with X...Cg [$(NH_2C_5H_3ClNH)^+(I)$] distances of 3.8520 Å (Fig. 4; Table 4).

Hirshfeld surface analysis

In the present research, we used not only Hirshfeld surfaces and 2D fingerprint plots, but also Crystal Explorer

(Spackman and Jayatilaka 2009), to identify intermolecular interactions and the environments of the components in the unit cell (two organic molecules, one isolated water molecule and one $[ZnBr_4]^{2-}$ anion).

The study of the cationic environment by Hirshfeld surface analysis

The Hirshfeld d_{norm} surface, shape index, curvedness and the 2D fingerprint plots of the cationic part in the $(NH_2C_5H_3ClNH)_2ZnBr_4 \cdot H_2O$ compound are depicted in Fig. 5. All interactions involving cationic parts in the crystal structure are displayed by the 2D fingerprint plots in Figs. 6 and 7. These analyses reveal the presence of different types of intermolecular interactions. It can be inferred that the dominant interactions are H...Br (25.1%), which are responsible for the appearance of deep red spots in the d_{norm} scheme. They are identified by N–H...Br and C–H...Br hydrogen bonds in the crystal lattice, where the molecules stand as donors ($d_e > d_i$). The second largest percentage (18.7%) can be attributed to the H...H interactions.
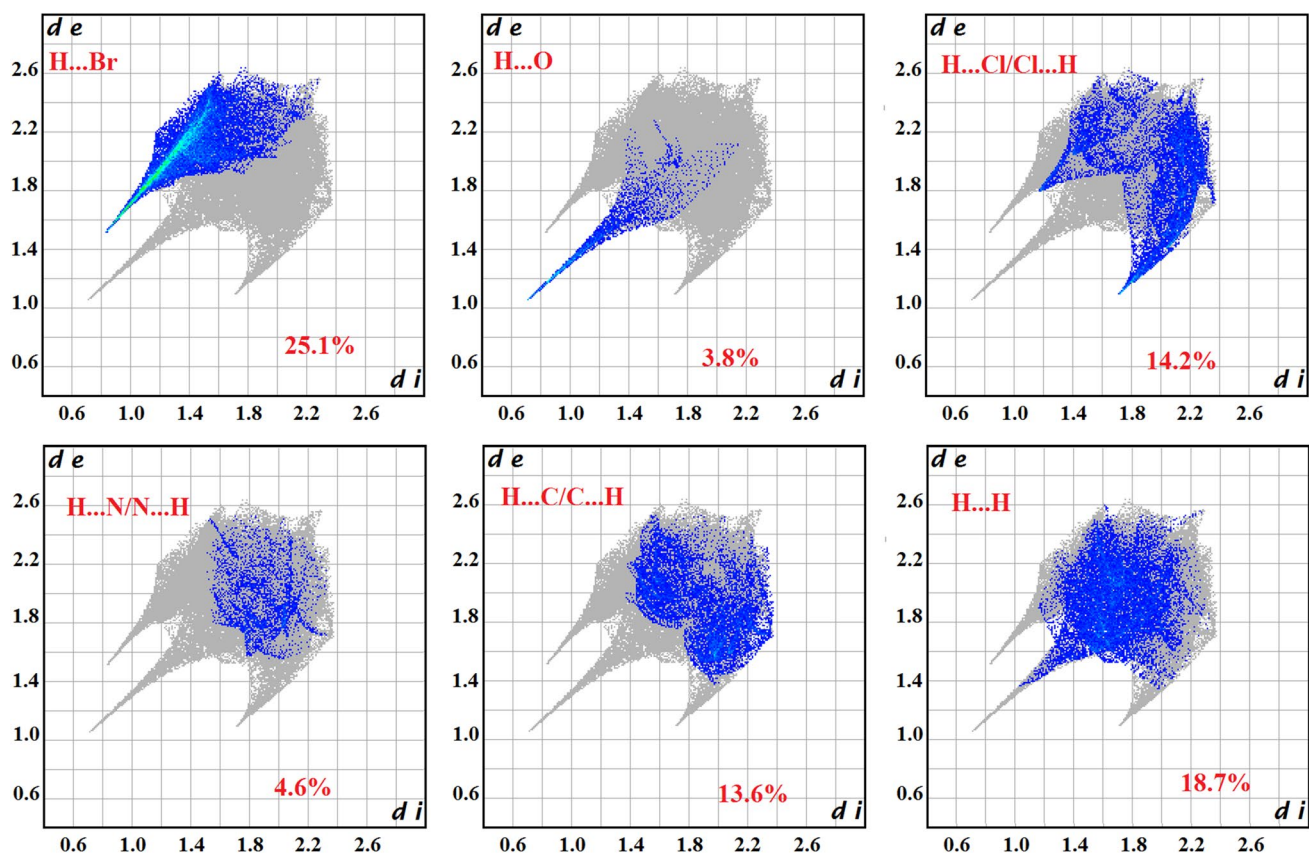
Fig. 6 Fingerprint plots resolved into different intermolecular interactions within the compound presenting percentages of contacts contributing to the Hirshfeld surface area of the cationic parts
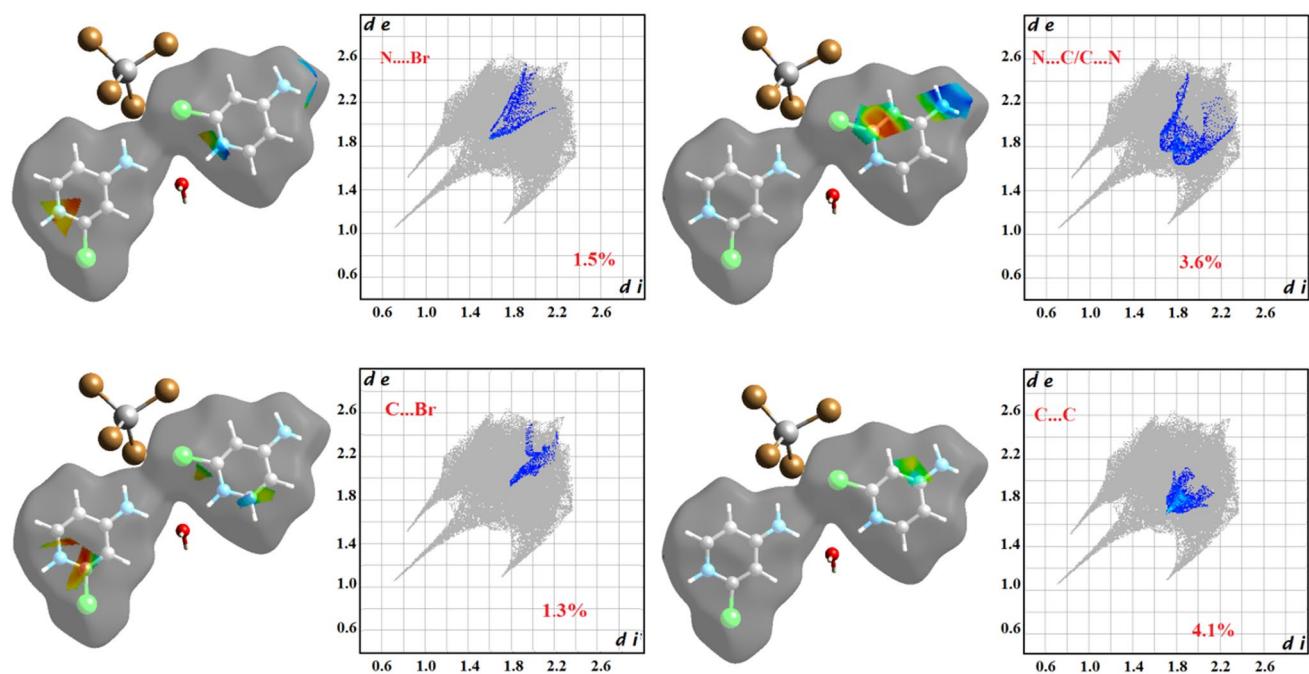

Fig. 7 Shape index and fingerprint plots resolved into $\pi\ldots\pi$ and $\pi\ldots$Br stacking interactions within the compound showing percentages contributing to the Hirshfeld surface area

Fig. 8 Hirshfeld surfaces of anionic part in the asymmetric unit of $(NH_2C_5H_3ClNH)_2ZnBr_4 \cdot H_2O$ compound, showing views of d_{norm} (**a**), shape index (**b**), curvedness (**c**), and 2D fingerprint plot (**d**)

d norm (a)

Shape index (b)

Curvedness (c)

Fingerpint plot (d)
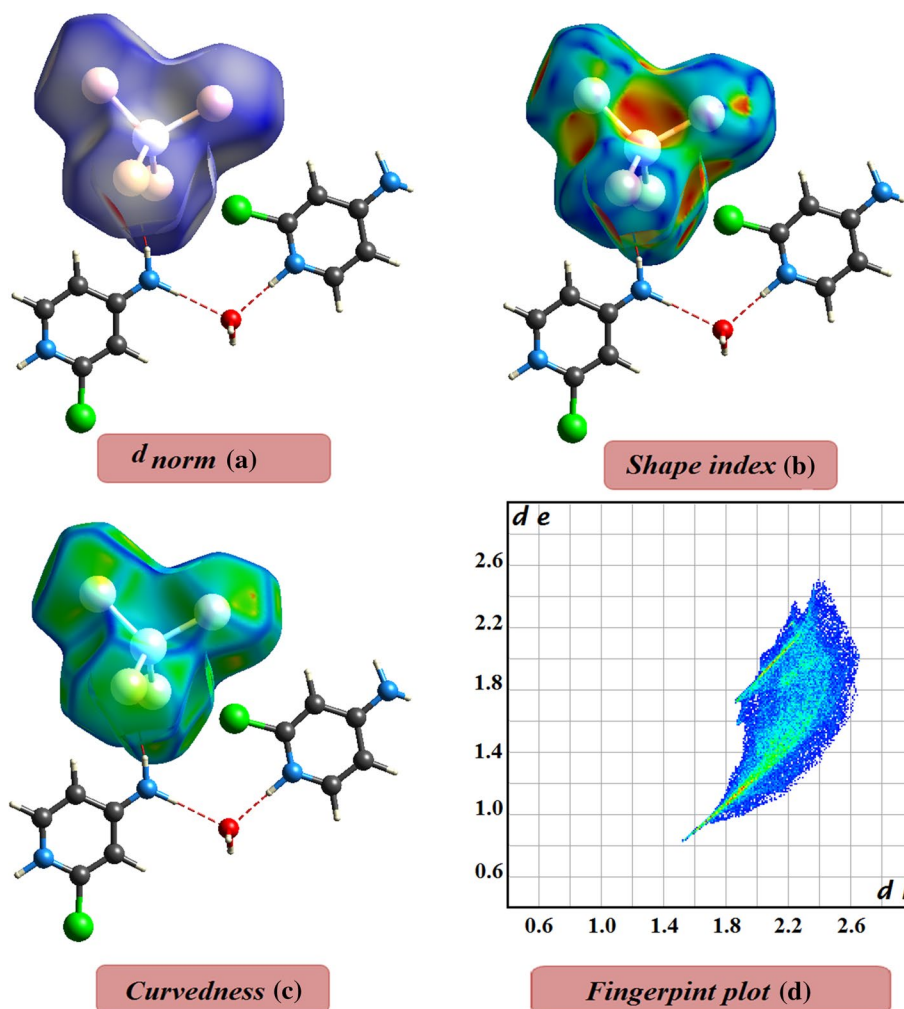
Additionally, it is interesting to note that intermolecular H…Cl/Cl…H interactions are not detected by X-ray analysis but through Hirshfeld surface analysis, which accounts for 14.2% of the organic cation (intramolecular interactions). The contribution of H…N/N…H, H…O and H…Cl/Cl…H contacts to the total Hirshfeld surface is relatively small; 4.6, 3.8, and 14.2%, respectively.

The H–H interactions, appearing in the middle of scattered points in the 2D fingerprint map, comprise 18.7% of the total Hirshfeld surfaces. Nevertheless, they are obvious, because the majority of the surface of this molecular crystal is covered by H atoms. This proves that *van der Waals* interactions exert an important influence on the stabilization of the crystal lattice packing. We can also report the presence of H…C/C…H close contacts, which appear in the middle in the 2D fingerprint plot comprising 13.6% of the total Hirshfeld surface of the cationic molecules.

The presence of the adjacent red and blue triangles on the shape index surface (surrounded by a black circle in Fig. 5b demonstrates the presence of π…Br and π–π stacking interactions, which exist between two pyridin rings of

the cationic part $[NH_2C_5H_3ClNH]^+$. This result has been confirmed by X-ray crystal structural analysis (Fig. 4).

Analysis of Hirshfeld surface shows the interactions between N…Br and C…Br with the percentages 1.5% and 1.3%, respectively of the Hirshfeld surface (Fig. 7). Again, very low percentages of N…C/C…N (3.6%) and C…C (4.1%) interactions are recorded in the molecule. Thus, π–π stacking interactions are not visible in the rotated d_{norm} map $([NH_2C_5H_3ClNH]^+(II))$ owing to the corresponding C…C distances between pyridin rings which are longer than the sum of *van der Waals* radii, as it can be perceived in crystal structure determination.

The study of the anionic environment by Hirshfeld surface analysis

The Hirshfeld surface analysis of $[ZnBr_4]^{2-}$ is displayed in Fig. 8, exhibiting the surfaces that have been mapped around the molecule by d_{norm}, shape index, curvedness and 2D fingerprint plots.
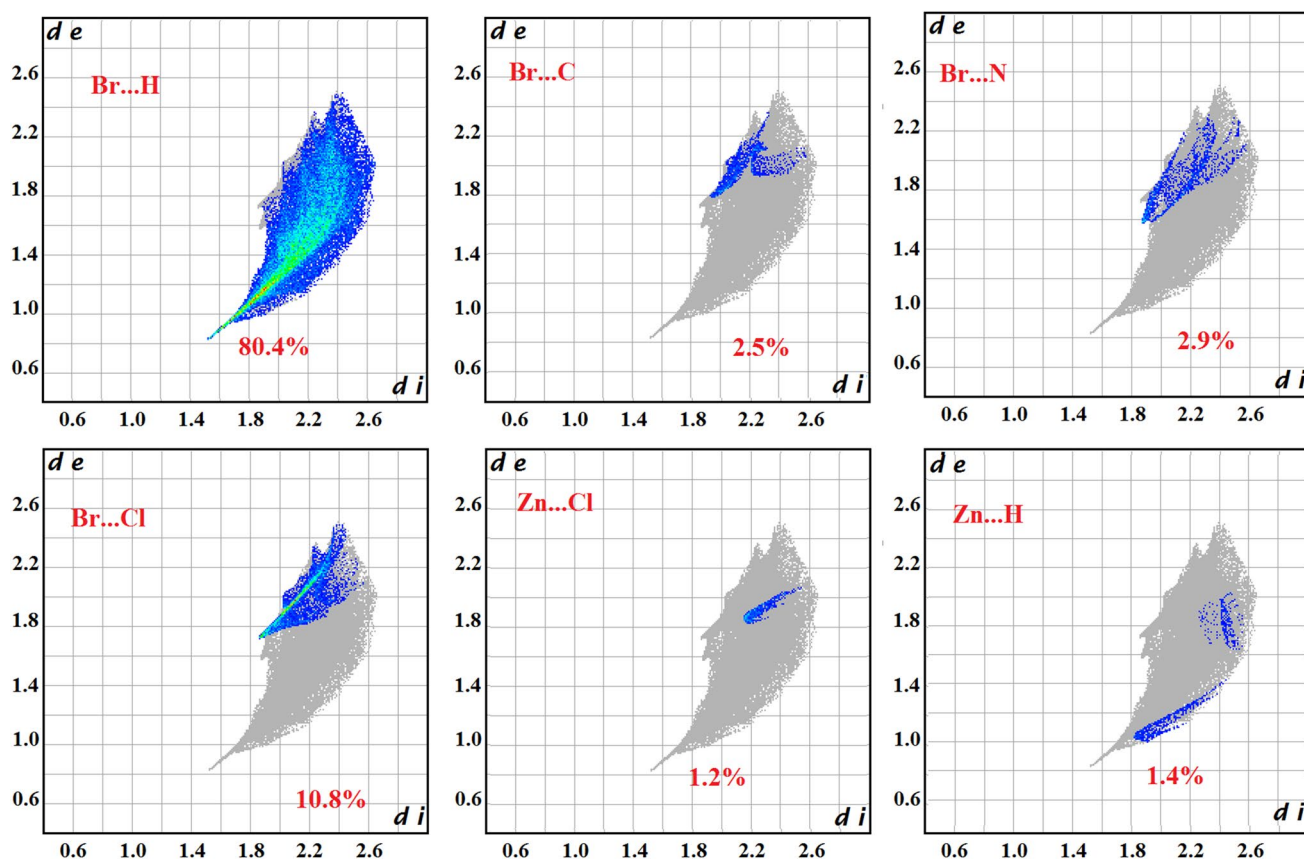
Fig. 9 Fingerprint plots resolved into different intermolecular interactions within the $(NH_2C_5H_3ClNH)_2ZnBr_4 \cdot H_2O$ compound showing percentages of contacts contributing to the Hirshfeld surface area of the anionic part

The decomposed fingerprint plots (Fig. 9) show that the intermolecular Br…H contacts present a major contribution to the anionic environment (80.4%), displaying a large circular depression on the d_{norm} surface. These contacts are visible in the fingerprint where one $[ZnBr_4]^{2-}$ acts as an acceptor ($d_i > d_e$). Other visible spots in the Hirshfeld surfaces attributed to Br…Cl, are detected by a spike in the top left region of its corresponding fingerprint ($d_e = 2.00\,\text{Å}$, $d_i = 2.00\,\text{Å}$). Br…C and Br…N interactions participate in overall interactions with 2.5 and 2.9%, respectively.

The study of the water molecule environment by Hirshfeld surface analysis

Intermolecular contacts were analyzed around the water molecule in the asymmetric unit. The Hirshfeld surface analysis of the water molecule is depicted in Fig. 10, which is mapped by d_{norm}, shape index, curvedness and the 2D fingerprint plots. Figure 11 illustrates the decomposing of fingerprint plot. It is clear that H…H contacts are the most important interactions (30.9%), which refer basically to

the abundance of hydrogen on the molecular surface. The H…O/O…H presents the next most abundant contacts. The proportion of these interactions comprises 28.5% of the total Hirshfeld surfaces for a water molecule.

The wings at the top left ($d_i < d_e$) correspond to the points on the surface around the O–H donor characteristic of O–H…Br. H…Cl interactions. The decomposition of the fingerprint plot shows that H…Br contacts correspond to 28.5% of the total Hirshfeld surface area for the molecule. The H…Cl interactions contribute to only 8.4% of the Hirshfeld surface.

Vibrational frequencies of the FT-IR spectroscopy

To gain more information on the crystal structure, an FT-IR spectroscopy study was performed at room temperature between 4000 and 400 cm^{-1} (2.5–25 μm). IR spectrum is shown in Fig. 12, and its corresponding assignments are depicted in Table 5. IR-spectroscopy has been successfully used in analysis and identification of the fundamental vibrations and associated rotational–vibrational structure. It is

Fig. 10 Fingerprint plots resolved into different intermolecular interactions within the $(NH_2C_5H_3ClNH)_2ZnBr_4 \cdot H_2O$ compound showing percentages of contacts contributing to the Hirshfeld surface area of the water molecule

d_{norm} **(a)**

Shape index **(b)**

Curvedness **(c)**

Fingerpint plot **(d)**
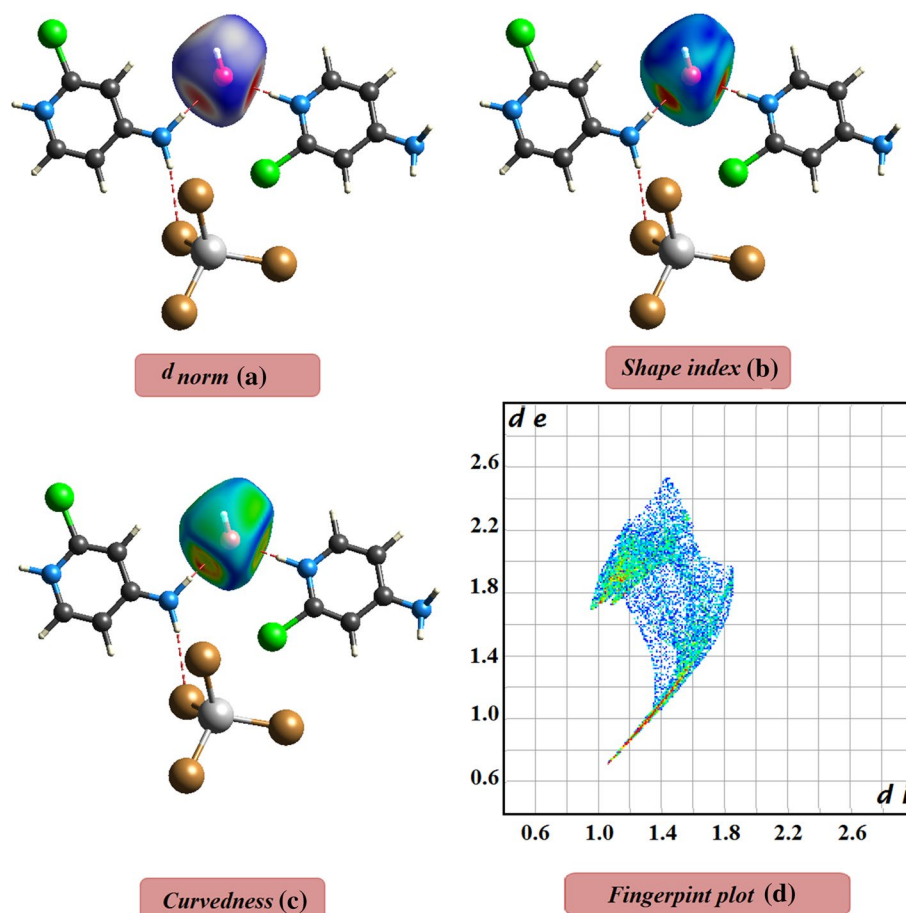
very difficult to attribute the vibration modes to organic and inorganic groups, the uses of analogous compounds are very necessary.

We used the spectrum of free 4-amino-2-chloropyridine $[NH_2C_5H_3ClN]$ when assigning the FT-IR vibrational frequencies of the organic groups of the title compound bis (4-amino-2-chloropyridinium) tetrabromozincate(II), $(NH_2C_5H_3ClNH)_2ZnBr_4 \cdot H_2O$.

Based on FT-IR studies performed on compounds having similarities with our compound (Karaa et al. 2010, 2012, 2013), different bands for the observed organic groups (N–H), (NH_2) C–N, C–N–C and C–Cl groups were assigned. Figure 12 shows the FT-IR spectra of the two compounds at room temperature.

Vibration of NH$_2$ group The asymmetric vibrations of NH$_2$ groups are observed in FT-IR spectrum as weak bands in the range 3300 cm^{-1} and the symmetric stretching vibrations of NH$_2$ groups are observed in FT-IR around 3196 cm^{-1} for the $(NH_2C_5H_3ClNH)_2ZnBr_4 \cdot H_2O$. The bands at 1646 cm^{-1} in FT-IR are assigned to NH$_2$ scissoring mode and the NH$_2$ twisting and wagging bands are observed in the range 990–552 cm^{-1}.

Vibration of NH group In the FT-IR, it is also interesting to indicate that v(N–H) mode appears at 3196 cm^{-1}

for $(NH_2C_5H_3ClNH)_2ZnBr_4 \cdot H_2O$ (and not observed in $[NH_2C_5H_3ClN]$). The δ(N–H) bending vibration of the N–H group appears at 1582 cm^{-1} for $(NH_2C_5H_3ClNH)_2ZnBr_4 \cdot H_2O$ (and not observed in $[NH_2C_5H_3ClN]$). This result confirms that C–N–C groups of 4-amino-2-chloropyridinium cation are protonated. The protonation of the pyridine ring produces dramatic changes in frequencies observed for bands originating from vibrations of ring.

Vibrations of water molecules

The band characteristics of water molecules exist at about 3758 and 3516 cm^{-1}.

Vibrations of C–N, C–C, C–N–C and N–C–N groups Hence, in the present investigation, FT-IR bands observed at 1364 and 1414 cm^{-1} of $(NH_2C_5H_3ClNH)_2ZnBr_4 \cdot H_2O$ are assigned to the side chain (C–N) stretching mode of vibrations. By referring to the above literature value (4-amino-2-chloropyridine), the bands that appear at 1528-1512 cm^{-1} in the FT-IR spectrum of the $(NH_2C_5H_3ClNH)_2ZnBr_4 \cdot H_2O$ are assigned to stretching (C–C) vibrations. The C–N–C and C–C–C out-of-plane and C–N–C and C–C–C in-plane bending vibrations are strongly coupled vibrations

Fig. 11 Fingerprint plots resolved into different intermolecular interactions within the $(NH_2C_5H_3ClNH)_2ZnBr_4 \cdot H_2O$ compound showing percentages of contacts contributing to the Hirshfeld surface area of the water molecule

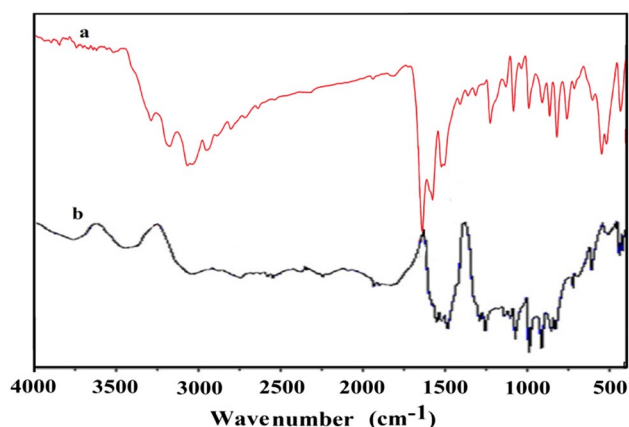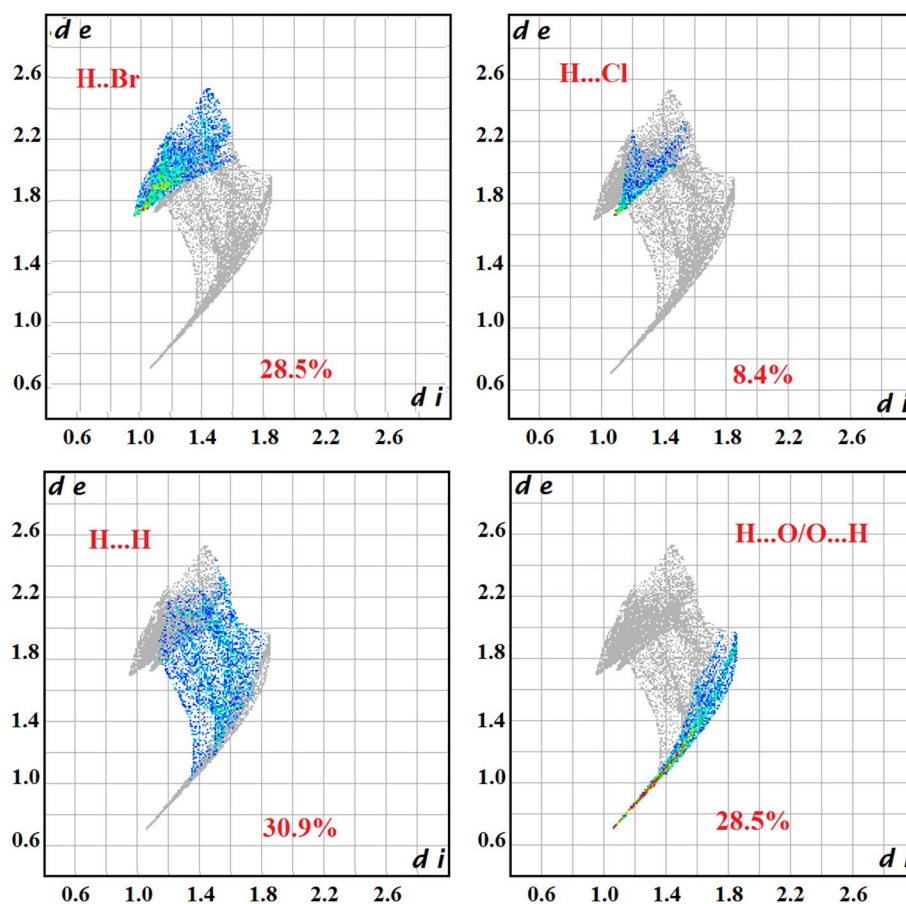**Fig. 12** FT-IR spectra of **a** $(NH_2C_5H_3ClNH)_2ZnBr_4 \cdot H_2O$ and **b** $[NH_2C_5H_3ClN]$ at room temperature

and occur in the region between 552 and 436 cm^{-1} for the $(NH_2C_5H_3ClNH)_2ZnBr_4 \cdot H_2O$.

Impedance analysis

Impedance spectroscopy experiments were carried out in the frequency range between 209 Hz and 5 MHz at different temperatures 298 K $\leq$ T $\leq$ 438 K. The impedance spectra for $(NH_2C_5H_3ClNH)_2ZnBr_4 \cdot H_2O$ sample at several different temperatures are plotted in Fig. 13, elucidating the presence of a single semicircle arc, which indicates departure from the Cole–Cole behavior (Nefzi et al. 2013).

The variation of real (Z') and imaginary (Z'') parts of impedance with frequency at various temperatures are depicted in Fig. 14a, b. In the higher frequency region ($> 10^4$ Hz), the merging of real part of the impedance curves can be attributed to the exit of space charge (James and Srinivas 1999; Selvasekarapandian and Vijaykumar 2003). Furthermore, the frequency dependence of the imaginary (Z'') parts of impedance at several temperatures show that Z'' values achieve a maximum (Z''_{max}), shifting to higher frequencies with increasing temperature. This conductivity marks the presence of relaxation in the system.

Dielectric studies

The mechanisms of conductivity of the materials have been investigated using the dependence of the frequency on electrical conductivity. Besides, the dielectric relaxation studies are of extreme significance in terms of specifying the nature and the origin of dielectric losses, which in turn may

Table 5 Assignments of FT-IR wavenumbers in the range 4000–400 cm^{-1}

Band assignment (cm^{-1})	[NH$_2$C$_5$H$_3$ClN]	(NH$_2$C$_5$H$_3$ClNH)$_2$ZnBr$_4$·H$_2$O
ν_{as} (OH)	–	3758
ν_s (OH)	–	3516
ν_{as} (NH$_2$) + ν (C–H)	3445	3402
ν_{as} (NH$_2$)	3366	3300
ν_{as} (N–H)		3196
ν (C–H) + ν_s (N–H)	3152	3071–3046
δ (NH$_2$)$_{scissoring}$	1656	1646
β (NH)$_{Balancement}$	–	1582
ν (C–C)$_{stretching}$	1552	1528–1512
ν (C–N)$_{stretching}$	1485	1414 vs
ν (C–N)$_{stretching}$	1416	1364
ν (C–NH$_2$)	1286	1228
t (NH$_2$)	988	990
γ (C–H)	828	824
γ (C–C)	722	762
ν (C–Cl)$_{stretching}$	608	608
ω(NH$_2$), γ(C–C–C)	518	552
β (C–C–C) β (C–H), β (C–N–C)	439	436

ν Stretching, β in-plane bending, γ out-of-plane bending, δ scissoring, ω wagging, t twisting, s symmetric vibrations, as antisymmetric vibrations
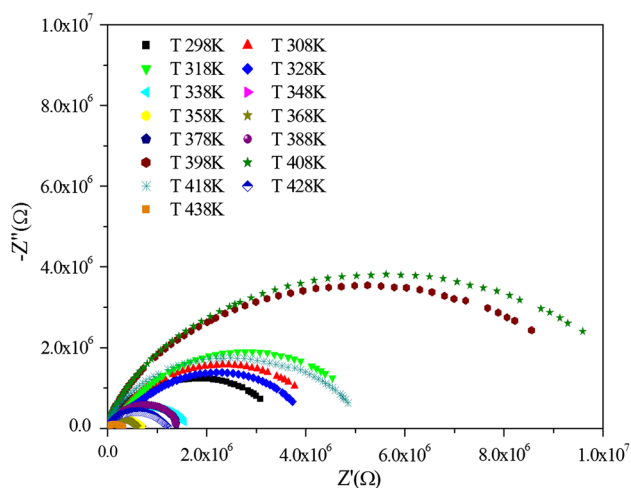
Fig. 13 Cole–Cole plots of the (NH$_2$C$_5$H$_3$ClNH)$_2$ZnBr$_4$·H$_2$O compound at several temperatures

be useful in the determination of the structure. The complex dielectric function is expressed as (Böhmer et al. 1993; Hodge et al. 2005):

$$\varepsilon^*(\omega) = \varepsilon' - j\varepsilon'',$$

where ε' and ε'' are the real and imaginary parts of the dielectric constant, respectively.

Figure 15a, b show the variation of the real ε' and imaginary ε'' parts of the dielectric constant as a function of frequency at several temperatures. It is clear from theses

plots that the values of ε' and ε'' decrease with increasing frequency at various temperatures, while they remain nearly constant at sufficiently high frequencies. Then, the high values at low frequencies can be attributed to the possible interface polarization mechanisms since interface states cannot follow the electric conductivity (ac) signal at high frequencies (Parlakturk et al. 2008; Park et al. 1998). Interface polarization reaches a constant value owing to the fact that beyond a certain frequency of the external field, the electron hopping cannot follow the alternative field. The resulting dispersions in ε' and ε'' with frequency may be assigned to Maxwell–Wagner (Bidault et al. 1994) and space charge polarization (Fanggao et al. 1996).

Temperature dependence of the real part ε' and the imaginary part ε'' of the dielectric constant are illustrated in Fig. 16a, b, which are measured at selected frequencies 1, 5, 10, 15 and 100 kHz. It is inferred from these evaluations, the presence of three anomalies localized at $T = 328, 380$ and 418 K, respectively. These evaluations confirm the results found by the simultaneous calorimetric study (DSC) and thermogravimetric analysis (TGA), which are reported in Fig. 17. The first peak signals the evaporation of water surface, while the second signal indicates the evaporation of water structure. The anomaly detected at $T = 418$ K may be associated with the phase transition (not detected in TGA), which is connected to the movement and the dynamic disorder of cationic parts. It should be also noted that the dielectric and thermal properties of our novel compound are very similar to those of the isostructural compound (Karâa et al. 2013).

Fig. 14 Variation of real (**a**) and imaginary (**b**) parts of impedance as a function of frequency at several temperatures
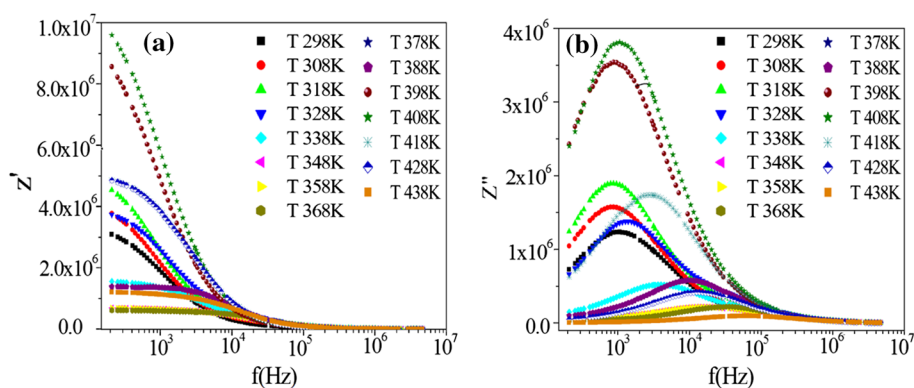

Fig. 15 The variation of the real ε' and imaginary ε'' parts of the dielectric constant as a function of frequency at several temperatures
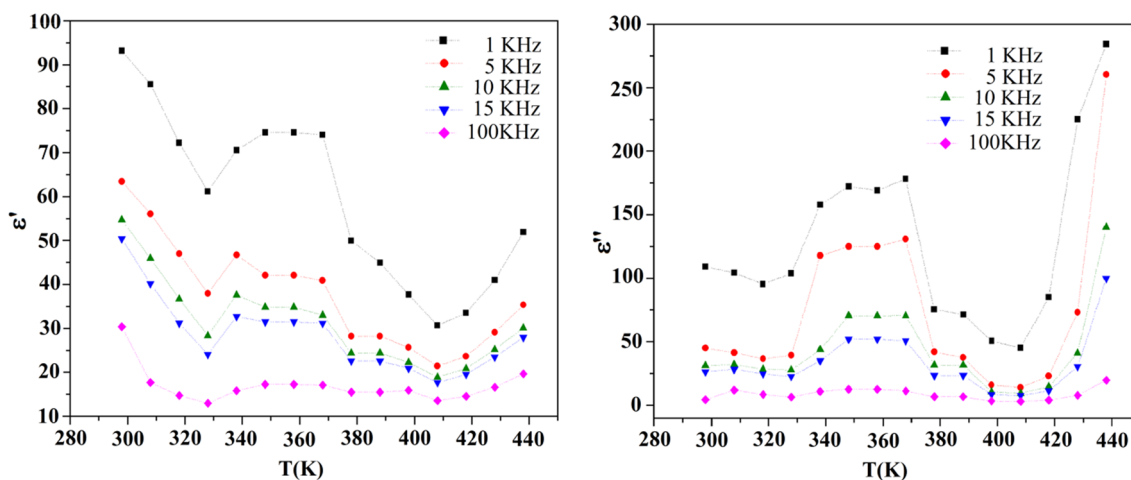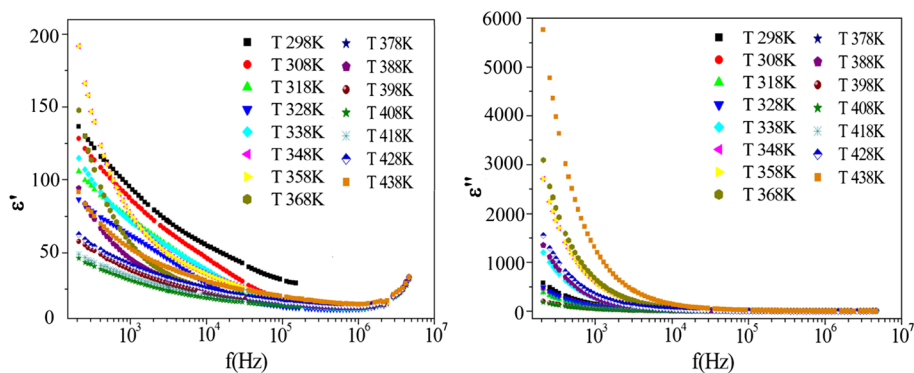
Fig. 16 Temperature dependence of the real ε' and imaginary ε'' parts of the dielectric constant at several frequencies

Conductivity analysis

The log–log plot of the electrical conductivity (σ_{ac}) versus frequency at different temperatures of $(NH_2C_5H_3ClNH)_2ZnBr_4 \cdot H_2O$ compound is exhibited in Fig. 18. Departing from this plot, we notice the presence of four distinct regimes. The $\sigma_{ac}(f)$ curves are found to be merging suggesting less defect mobility and low conductivity in the material. The phenomenon of the conductivity dispersion

in the materials is generally analyzed using Jonscher's power law (Jonscher 1999):

$$\sigma_{ac}(\omega) = \sigma_{dc} + A\omega^n,$$

where σ_{dc} is the frequency independent conductivity which can be obtained by extrapolating the low frequency plateau to zero frequency, A is a constant that depends on temperature and determines the strength of polarization and n is an exponent less than or equal to unity which represents the

Fig. 17 DSC-TGA runs at a rate of 5 K/min on heating (NH$_2$C$_5$H$_3$ClNH)$_2$ZnBr$_4$·H$_2$O compound
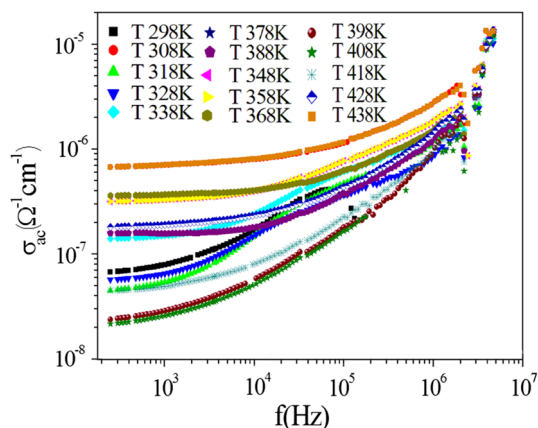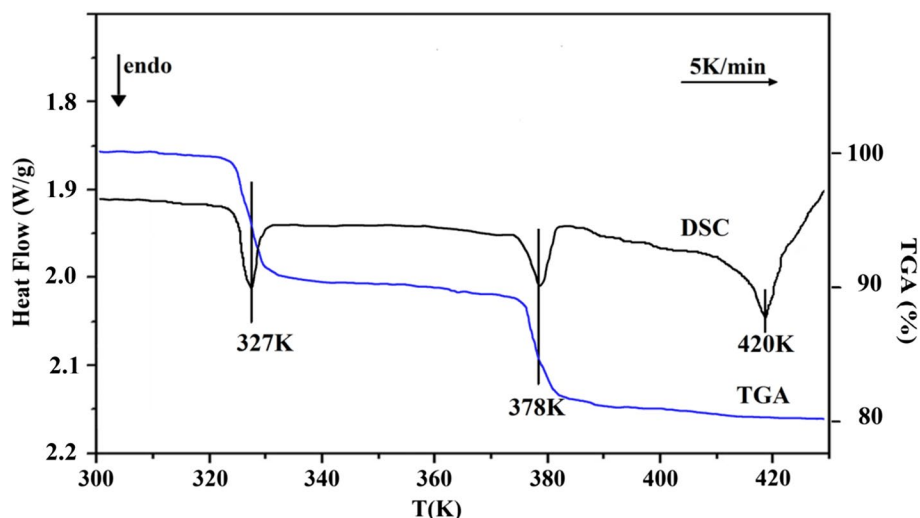
Fig. 18 Temperature dependence of the electrical conductivity (ac) at different frequencies

degree of interaction between mobile ions and its surrounding lattices (Dyre and Schrøder 2000).

In Fig. 19, conductivity data (dc) is represented in Arrhenius format as ln(σ_{dc}) versus 1000/T showing Arrhenius-type behavior that is described by:

$$T\sigma_{dc} = B\exp(-E_a/KT),$$

where B is the pre-exponential factor, E_a is the activation energy, and K is the Boltzmann's constant. This curve indicates the presence of four linear regions on each side of the anomalies ($T = 324$, 380 and 416 K). This behavior is in agreement with the previously observed DSC curve. The values of the activation energies determined only in the two regions II and IV are 0.3 and 0.4 eV, respectively. Based on thermal analysis results (DSC and ATG) and referring to the bibliography (Weng et al. 2011; Mesbeh et al. 2016; Karâa et al. 2010; 2012), we realize that the first region in temperature range 298–324 K corresponds to the beginning of evaporation of water surface, which is activated as soon as the heating has started. Region II in the temperature range 324–380 K corresponds to the ionic–protonic conduction. The value of the activation energy results in the hopping of proton H$^+$. Region III in the temperature range 380–416 K was detected also in the thermal property by TGA and DSC technical which could be accounted for the disappearance of the water molecule of the structure (construction water) and finally the region IV in the temperature range 416–438 K may refer to electronic conduction which will be more and more activated.

Fig. 19 Variation of ln($\sigma_{dc}T$) versus 1000/T of (NH$_2$C$_5$H$_3$ClNH)$_2$ZnBr$_4$·H$_2$O compound

Conclusion

To sum up, in this research work a novel Zn(II) hybrid compound has been synthesized and structurally characterized. The most prominent features of our structure refer basically to the presence of zero-dimensional (0D) anionic network built up of organic parts and water molecules. Hirshfeld surface analysis shows different types of intermolecular interactions including hydrogen bonding, and π–π(Cg–Cg) stacking and Zn–Br…Cg interactions. This paper highlights the usefulness of the Hirshfeld analysis in terms of understanding the intricacies of interactions occurring in crystallized solids.

Differential scanning, calorimetric and electric measurements were carried out. They showed the evaporation of water surface at the temperature range 298–324 K and structural water structural (construction water) at the temperature range 380–416 K. The activation energy issued from the impedance spectra suggests an ionic–protonic conductivity for this material. It is assigned by the mechanism of hopping in the temperature range 416–438 K which may be due to electronic conduction which will be more and more activated.

The value of the activation energy reveals a significant electrical property of the molecule confirming that this material is a good candidate to superconductor applications in energy conversion, miniaturized sensors and imaging devices, solar cells, LED and detectors.

References

Böhmer R, Ngai KL, Angell CA, Plazek DJ (1993) Nonexponential relaxations in strong and fragile glass formers. J. Chem. Phys. 99:4201–4209. https://doi.org/10.1063/1.466117

Bidault O, Goux P, Kchikech M, Belkaoumi M, Maglione M (1994) Space charge relaxation in perovskites. J Phys Rev B 49:7868–7873. https://doi.org/10.1103/physrevb.49.7868

Brandenburg K (1998) Diamond version 2.0 impact GbR. Bonn, Germany

Chihaoui N, Hamdi B, Salah AB, Zouari R (2016a) A new mononuclear complex: structure, vibrational (FT-IR and Raman), Hirshfeld surfaces analysis, electrical properties and equivalent circuit. J Phys Chem Biophys 6:216–226. https://doi.org/10.4172/2161-0398.1000216

Chihaoui N, Hamdi B, Dammak T, Zouari R (2016b) Molecular structure, experimental and theoretical spectroscopic characterization and non-linear optical properties studies of a new non-centrosymmetric hybrid material. J Mol Struct 1123:144–152. https://doi.org/10.1016/j.molstruc.2016.06.031

Chihaoui N, Hamdi B, Zouari R (2016c) Structural study, intermolecular interactions in view of X-ray and Hirshfeld surface analysis,

DSC characterization, and electrical properties of bis-(4-benzylpyridinium) tetrabromozincate. J Ionics 23:1173–1186. https://doi.org/10.1007/s11581-016-1926-4

Chihaoui N, Hamdi B, Zouari R (2017) Structural study, spectroscopic analysis and dielectric proprieties of new hybrid organic-inorganic compound. J Mol Struct 1147:48–55. https://doi.org/10.1016/j.molstruc.2017.06.087-&gt

Dyre JC, Schrøder TB (2000) Universality of ac conduction in disordered solids. J Rev Modern Phy 72:873–892. https://doi.org/10.1103/revmodphys.72.873

Farrugia LJ (1997) ORTEP-3 for Windows - a version of ORTEP-III with a Graphical User Interface (GUI). J Appl Crystallogr 30:565. https://doi.org/10.1107/S0021889897003117

Farrugia LJ (1999) WinGX suite for small-molecule single-crystal crystallography. J Appl Crystallogr 30:837–838. https://doi.org/10.1107/s0021889899006020

Fanggao C, Saunders GA, Lambson EF, Hampton RN, Carini G, Di Marco G, Lanza M (1996) Temperature and frequency dependencies of the complex dielectric constant of poly(ethylene oxide) under hydrostatic pressure. J Polym Sci: Part B: Polym Phys 34:425–433. https://doi.org/10.1002/(SICI)1099-0488(19960 2)34:3%3c425::AID-POLB%3e3.0.CO;2-S

Gao FX, Gu W, Yang YS, Qian J, Yan SP (2007) Bis(tetra-n-butylammonium) tetrabromidozincate (II). J Acta Cryst E 63:m1621. https://doi.org/10.1107/s160053680702140x

Gillon AL, Lewis GR, Orpen AG, Rotter S, Starbuck J, Wang X-M, Rodriguez-Martin Y, Ruiz-Pérez C (2000) Organic–inorganic hybrid solids: control of perhalometallate solid state structures. J Chem Soc Dalton Trans. https://doi.org/10.1039/b005036i

Hodge IM, Ngai KL, Moynihan CT (2005) Comments on the electric modulus function. J Non-Cryst Solids 351:104–115. https://doi.org/10.1016/j.jnoncrysol.2004.07.089

James AR, Srinivas K (1999) Low temperature fabrication and impedance spectroscopy of PMN-PT ceramics. J Mater Res Bull 34:1301–1310. https://doi.org/10.1016/s0025-5408(99)00127-0

Jonscher AK (1999) Dielectric relaxation in solids. J Phys D Appl Phys 32:R57–R70. https://doi.org/10.1088/0022-3727/32/14/201

Karaa N, Hamdi B, Ben Salah A, Zouari R (2012) Synthesis, infrared, MAS-NMR characterization, structural study and electrical properties of the new compound [C5H6ClN2]2Cd3Cl8. J Mol Struct 1013:168–176. https://doi.org/10.1016/j.molstruc.2011.12.053

Karâa N, Hamdi B, Oueslati A, Ben Salah A, Zouari R (2010) Preparation, infra-red, MAS-NMR and structural characterization of a new copper based inorganic–organic hybrid compound: [C5H6N2Cl]2CuCl4. J Inorg Organomet Polym 20:746–754. https://doi.org/10.1007/s10904-010-9409-y

Karâa N, Hamdi B, Ben Salah A, Zouari R (2013) Synthesis, infra-red, CP/MAS-NMR characterization, structural study and electrical properties of the bis(4-amino-2-chloropyridinium) tetrachlorozincate (II) monohydrate. J Mol Struct 1049:48–58. https://doi.org/10.1016/j.molstruc.2013.06.003

Koenderink JJ, van Doorn AJ (1992) Surface shape and curvature scales. Image Vis Comput 10:557–564. https://doi.org/10.1016/0262-8856(92)90076-f

Mesbeh R, Hamdi B, Zouari R (2016) (H2pdcCuBr 2)2•2(MH+)2Br−(M=Melamine, H2pdc=Pyridine-2,6-Dicarboxylic Acid): crystal structure, Hirshfeld surface analysis, vibrational and thermal studies. J Inorg Organomet Polym 26:744–755. https://doi.org/10.1007/s10904-016-0371-1

Nefzi H, Sediri F, Hamzaoui H, Gharb N (2013) Electric conductivity analysis and dielectric relaxation behavior of the hybrid polyvanadate (H3N(CH2)3NH3)[V4O10]. J Mater Res Bull 48:1978–1983. https://doi.org/10.1016/j.materresbull.2013.02.003

Ninković DB, Janjić GV, Zarić SD (2012) Crystallographic and ab initio study of pyridine stacking interactions. Local nature of

hydrogen bond effect in stacking interactions. J Cryst Eng Commun 12:2113–2121. https://doi.org/10.1021/cg201389y

North ACT, Phillips DC, Mathews FS (1968) A semi-empirical method of absorption correction. Acta Cryst A24:351–359. https://doi.org/10.1107/S0567739468000707

Park BH, Hyun SJ, Moon CR, Choe BD, Lee J, Kim CY, Jo W, Noh TW (1998) Imprint failures and asymmetric electrical properties induced by thermal processes in epitaxial $Bi_4Ti_3O_{12}$ thin films. J Appl Phys 84:4428–4435. https://doi.org/10.1063/1.368666

Parlakturk F, Altındal S, Tataroglu A, Parlak M, Agasiyev A (2008) On the profile of frequency dependent series resistance and surface states in Au/$Bi_4Ti_3O_{12}$/SiO_2/n-Si(MFIS) structures. J Microelectron Eng 85:81–88. https://doi.org/10.1016/j.mee.2007.03.012

Selvasekarapandian S, Vijaykumar M (2003) The ac impedance spectroscopy studies on $LiDyO_2$. J Mater Chem Phys 80:29–33. https://doi.org/10.1016/s0254-0584(02)00510-2

Sheldrick GM (1997a) SHELXL-97. Program for crystal structures refinement, University of Gottingen. Electron Crystallogr. https://doi.org/10.1007/978-94-015-8971-0_18

Sheldrick GM (1997b) SHELXS-97. Program for the solution of crystal structures, University of Gottingen. Electron Crystallogr. https://doi.org/10.1007/978-94-015-8971-0_18

Spackman MA, Byrom PG (1997) A novel definition of a molecule in a crystal. J Chem Phys Lett 267:215–220. https://doi.org/10.1016/s0009-2614(97)00100-0

Spackman MA, Jayatilaka D (2009) Hirshfeld surface analysis. J Cryst Eng Commun 11:19–32. https://doi.org/10.1039/b818330a

Spackman MA, McKinnon JJ (2002) Fingerprinting intermolecular interactions in molecular crystals. J Cryst Eng Commun 4:378–392. https://doi.org/10.1039/b203191b

Spek AL (2003) Single-crystal structure validation with the program PLATON. J Appl Cryst 36:7–13. https://doi.org/10.1107/s0021889802022112

Weng DF, Wang BW, Wang ZM, Gao S (2011) Polymorphism of (H_2mela)$_2$[$CuCl_5$] Cl (mela = melamine): structures, transformation and magnetic properties. Cryst Eng Commun 13:4683–4688. https://doi.org/10.1039/c1ce05143a

Wheeler SE (2012) Understanding substituent effects in noncovalent interactions involving aromatic rings. Acc Chem Res 46(4):1029–1038. https://doi.org/10.1021/ar300109n

Wolff SK, Grimwood DJ, McKinnon JJ, Turner MJ, Jayatilaka D, Spackman MA (2012) CrystalExplorer 3.1. University of Western Australia, Crawley